RSC Advances

PAPER

View Article Online
View Journal | View Issue

Cite this: *RSC Adv.*, 2025, **15**, 49468

Effects of electrohydrodynamic parameters on printing ultra-fine low-resistivity silver electrodes

Huacheng Tang, [a] Honglong Ning, [ab] Rihui Yao, [ad] Zhenchao Li,*[ca] Zhaohui Li,[a] Zhenhuai Yang,[e] Qi Lu,[e] Qiang Hu,[e] Wei Xu *[a] and Junbiao Peng[a]

Received 29th October 2025
Accepted 3rd December 2025

DOI: 10.1039/d5ra08292g

rsc.li/rsc-advances

Electrodes, as signal transmission channels for microelectronic components, need to develop towards high precision. Among the existing printed electronic technologies, electrohydrodynamic (EHD) jet printing utilizes electric field force to control ink, enabling higher precision electrode processing. In this paper, the relationship between the printing parameters of EHD-printer and the morphology of the electrodes was investigated. With the decreasing of driving voltage and bias voltage, the line width of the silver electrode became more and more narrow. Silver electrodes with line width of 3.85 μm were fabricated through process optimization. In addition, with the annealing temperature rising, the resistivity of the electrode gradually decreased. The possible reason was that higher temperatures could not only increase the binding degree of silver nanoparticles, but also promote the removal of organic matter. Silver electrodes with resistivity of 13.63 μΩ cm were fabricated through process optimization, which showed an important application potential of the silver electrode printed by electrohydrodynamic inkjet printing.

1. Introduction

With the size of electronic device becoming smaller, electrodes, which serve as signal transmission channels, also need to develop towards greater precision. Electrohydrodynamic inkjet printing is a new inkjet printing technology that can be used to prepare high-precision electrodes,[1,2] does not require vacuum condition,[3] and is low cost.[4] The electro-hydrodynamic inkjet printing primarily consists of the electrohydrodynamic printer, the nozzle, and the printing ink.[5,6] As shown in Fig. 1(a), the voltage is applied between nozzle and substrate through power supply.[7,8] The electric field force (F_e) will make the ink form a Taylor cone at the nozzle.[9,10] There are various mechanisms explaining the formation of the Taylor cone.[11,12] As depicted in Fig. 1(b), when no additional voltage is applied to the nozzle, the printing ink, due to surface tension (F_s), forms a ellipsoidal droplet at the nozzle.[13] When a high voltage is applied between the nozzle and the substrate, the ink is stretched under the nozzle to form a Taylor cone. With the strength of the electric field increasing, the Taylor cone is further stretched and becomes unstable, resulting in ink separation and jet formation.[14,15]

Compared to traditional inkjet printing technologies, electro-hydrodynamic inkjet printing utilizes a wider range of inks,[16,17] including high-viscosity ink[18,19] and non-traditional ink,[20] such as bionutrient ink used for cell culture in the biomedical field.[21] Among the various types of conductive inks, silver nanoink has the advantages of lower resistivity and adjustable viscosity,[22] making it suitable for printing silver electrodes with extremely low resistivity.[23,24] Qi Lei *et al.* utilized an electrohydrodynamic printer combined with *in situ* active silver ink to print micro-patterned conductive silver electrodes, achieving a minimum size of 27.6 ± 3.4 μm with a conductivity of 3.3 × 10^6 S m^{-1}.[25] Hongfu Liang *et al.* optimized the EHD printing process, achieving a line width of 19.42 ± 0.24 μm and a conductivity of 6.01 × 10^6 S m^{-1} for silver electrodes.[26] Ding. Y *et al.* used integration of electro-hydrodynamic printing and hydroprinting to achieve a electrode line width with 10 μm.[27]

[a]*Guangdong Basic Research Center of Excellence for Energy & Information Polymer Materials, State Key Laboratory of Luminescent Materials and Devices, School of Materials Sciences and Engineering, South China University of Technology, Guangzhou 510640, China. E-mail: xuwei@scut.edu.cn*

[b]*The International School of Microelectronics, Dongguan University of Technology, Dongguan 523808, China*

[c]*State Key Laboratory of Advanced Materials and Electronic Components, Fenghua Electronic Industrial Park, No. 18 Fenghua Road, Zhaoqing 526020, China*

[d]*Key Lab of Guangdong Province for High Property and Functional Polymer Materials, South China University of Technology, Guangzhou 510640, China*

[e]*Ji Hua Laboratory, Foshan 528000, China*

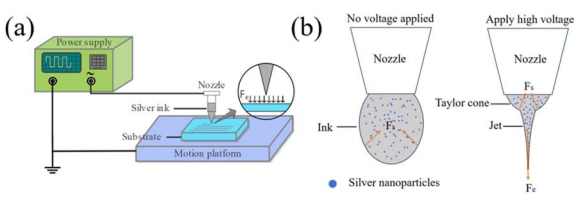

Fig. 1 Schematic diagram of electrohydrodynamic inkjet printing: (a) EHD inkjet printing model diagram; (b) jet of ink.

However, the use of electrohydrodynamic inkjet printing to fabricate silver electrodes still faces challenges such as the need for further reduction of line-width and resistivity.[28] In this paper, the relationship between the printing parameters and the morphology of silver electrodes was studied. In addition, the relationship between the annealing temperature and the resistivity of silver electrode was also studied.

2. Materials and methods

2.1 Materials

In this paper, the material of the substrate and nozzle were glass. The silver ink(40 LT-15C) used was purchased from ANP Company in South Korea. The solvent of the ink was triethylene glycol monoethyl ether, and the average particle size of the silver nanoparticles was 80 nm.

2.2 Preparation process

An electrohydrodynamic printer (SIJTechnology SIJ-S150, Tokodai, Ibaraki, Japan) was used to print electrodes in this paper. The preparation process of silver electrodes was divided into four steps: substrate cleaning, ink treatment, electrode printing and post treatment.

As shown in Fig. 2, in the substrate cleaning, the glass substrate is placed in beakers containing deionized water and isopropanol in turn for ultrasonic treatment. In the ink treatment, the ink is treated by ultrasonic to prevent particles from gathering and causing nozzle blockage. In the above steps, the power of ultrasonic treatment is 200 W, the time is set to 15 min, and the temperature is set to 25 °C. After configuring the printing parameters, silver electrodes are printed. After printing, the electrode needs to be treated at 60 °C for 10 minutes and then at the set high temperature for 20 minutes.

2.3 Test

In this paper, the contact angle between the silver ink and the glass substrate was measured by a tensiometer (Theta Lite 200). The contact angle was measured using the sessile drop method, and the surface tension of the ink was measured using the pendant drop method. The viscosity of silver ink was tested by a three-segment shear program on a rotary rheometer (HAAKE Mars 40).

The line width and cross-sectional area of the silver electrodes were measured by a laser confocal microscope (OLYMPUS LEXT OLS 5000). The uniformity of the electrode line width was calculated using the following formula (1):

$$\text{Uniformity} = \frac{L_{\max} - L_{\min}}{L_{\max} + L_{\min}} \times 100\% \quad (1)$$

where $L_{\max}$ is the maximum line-width of the electrode. Where $L_{\min}$ is the minimum line-with of the electrode. The smaller the value of uniformity is, the more uniform the electrode linewidth is.

The *I–V* curve of the silver electrode was measured by a semiconductor parameter analyzer (Primarius FS Pro, PX500, Pudong New Area, Shanghai, China) to fit the electrode resistance. The resistivity of the silver electrode can be obtained using the following formula (2):

$$\rho = R\frac{S}{L} \quad (2)$$

where R is the resistance of the electrode, S is the cross-sectional area of the electrode, and L is the length of the electrode fixed at 1 mm.

2.4 Statistical analysis

Each experiment above involved five replicates. This ensures that the data has high repeatability. Data on line width and resistivity are presented as the means ± standard deviations. In the graphs, vertical bars represent the mean, and the error bars represent the standard deviation.

3. Results and discussion

3.1 Ink properties

According to the three-segment shear viscosity test results of silver ink, the viscosity of silver ink was 6.8 cps at 25 °C. Fig. 3(a) shows that the surface tension of silver ink was 74.9 mN m^{-1}. Fig. 3(b) shows the contact angle test between the silver ink and a glass substrate. The average contact angle between ink and substrate was 20.885° ± 0.225°.

3.2 Morphology of silver electrodes

3.2.1 Voltage waveform

3.2.1.1 Driving voltage. Fig. 4 shows the electrode morphology under different driving voltages. With the driving voltage increasing, the amount of ink ejected became more and more, resulting in an enhanced ink spreading effect.

Fig. 5 shows the effect of driving voltage on the line width and cross-sectional area of silver electrodes. With the driving voltage decreasing from 240 V to 130 V, the line width of electrode decreased from 10.51 μm to 3.85 μm, and the cross-sectional area of electrode decreased from 0.74 μm^2 to 0.33

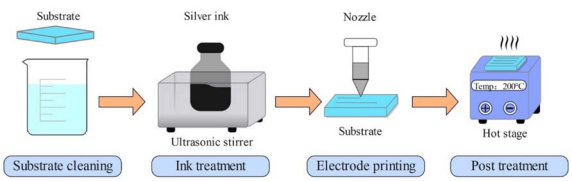

Fig. 2 Preparation process for silver electrodes.

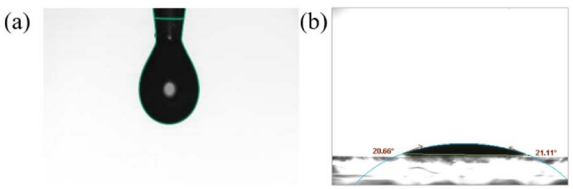

Fig. 3 Ink properties: (a) surface tension; (b) the contact angle of silver ink on glass substrate.

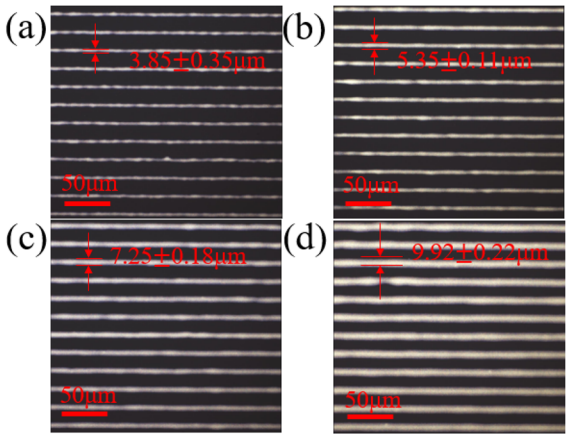

Fig. 4 Electrode morphology images under different driving voltages: (a) 130 V; (b) 160 V; (c) 190 V; (d) 220 V.

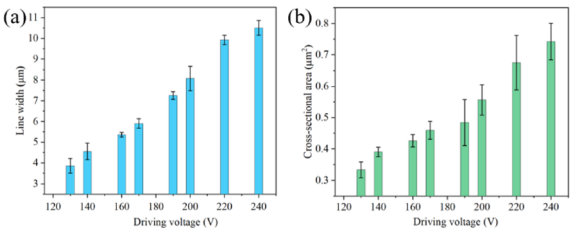

Fig. 5 The effect of driving voltage on silver electrodes:(a) line width; (b) cross-sectional area.

μm^2. The possible explanation was that, the strength of electric field formed between the nozzle and the substrate decreased with the driving voltage decreasing.[29] The reduction of electric field force made the ink droplets ejected from the Taylor cone smaller, resulting in the reduction of linewidth and cross-sectional area.

3.2.1.2 Bias voltage. Fig. 6(a) shows the voltage waveforms before and after applying a bias voltage. The bias voltage is a compensation voltage for the driving voltage. After applying a bias voltage of 240 V on the basis of a driving voltage of 200 V,

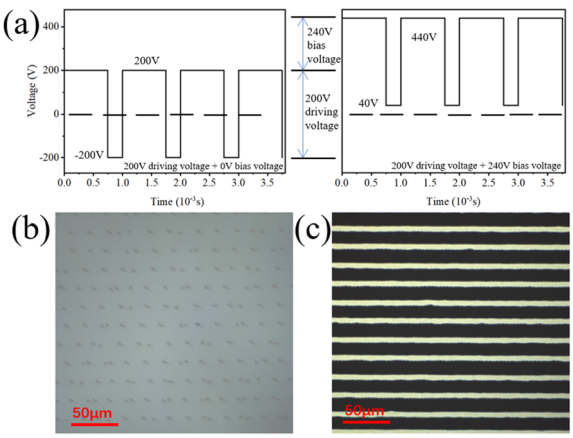

Fig. 6 The effect of bias voltage on electrode morphology: (a) voltage waveform before and after applying bias voltage; (b) no bias voltage; (c) bias voltage of 240 V.

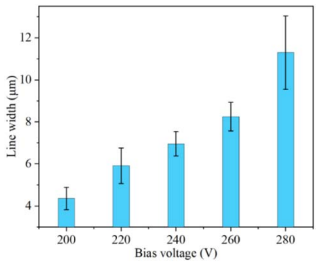

Fig. 7 The effect of bias voltage on the linewidth of silver electrodes.

the high level applied to the nozzle rises from 200 V to 440 V, and the low level rises from −200 V to 40 V. Fig. 6 (b) and (c) show the effect of bias voltage on electrode morphology. Only very small ink droplets were printed when no bias voltage was applied. In contrast, complete electrode line was printed when an appropriate bias voltage is applied. The application of bias voltage provided an additional electric field pulling force for the ink, which could shorten the time it took for the jet to form on one hand, and delay the rupture behavior of jet on the other hand.[30] This meant that a larger volume of ink drops was printed in one cycle, so that the complete electrode line was printed.

Fig. 7 shows the effect of bias voltage on the linewidth of silver electrodes. The line-width decreased from 11.30 μm to 4.35 μm with the bias voltage decreasing from 280 V to 200 V. When the bias voltage was 200 V, the standard deviation of the electrode line width was minimized. Similar to the driving voltage, the decrease in bias voltage led to a reduction in the electric field force at the nozzle, resulting in a decrease in the amount of ink ejected. Ultimately, it led to a reduction in electrode line width.

3.2.1.3 Waveform frequency. Fig. 8 shows the effect of waveform frequency on the linewidth of silver electrodes. In this paper, the linewidth of electrode first increased and then decreased with the waveform frequency increasing from 700 Hz to 1000 Hz. Compared to the linewidth average at 700 Hz, the linewidth average at 800 Hz is 19.74% larger, 12.59% larger at 900 Hz, and 8.83% larger at 1000 Hz. Compared to the driving voltage and bias voltage, the difference in electrode linewidth is not significant at different waveform frequencies. According to formula (1), the uniformity value of the electrode under

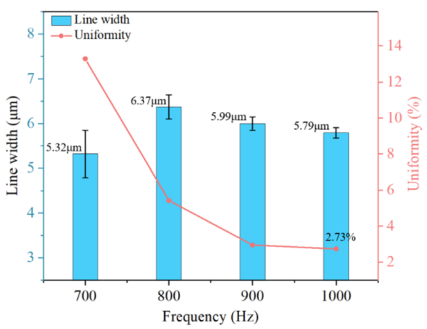

Fig. 8 The effect of waveform frequency on the linewidth of silver electrodes.

different waveform frequencies could be calculated. With the waveform frequency increasing, the uniformity value of the electrode linewidth gradually decreased, indicating that a higher waveform frequency contributed to a more uniform electrode linewidth. Notably, the silver electrode printed at a frequency of 1000 Hz had a linewidth of 5.79 μm, but the uniformity value was only 2.73%, indicating that the electrode linewidth was the most uniform. In fact, with the waveform frequency increasing, the duration of the high level correspondingly decreased in one voltage cycle, which reduced the jetting time. Under constant moving speed conditions, the reduction of jetting time would directly decrease the length of the electrode line segments printed in a single cycle.[31] Considering that the macro electrode was composed of multiple micro segments, reducing the length of micro segments would make the macro electrode linewidth more uniform.

3.2.2 Moving modes

3.2.2.1 Moving speed. Fig. 9 shows the effect of movement speed on the line width of silver electrodes. With the moving speed increasing from 5 mm s^{-1} to 30 mm s^{-1}, the electrode line width gradually decreased from 7.6 μm to 5.3 μm, indicating that the line width could be controlled by adjusting the moving speed. The main reason may be that the ink ejection volume is fixed under the same voltage conditions. The increase in movement speed causes the electrode line length to become longer, resulting in a decrease in line width.

3.2.2.2 Moving acceleration. Fig. 10 shows the effect of acceleration on the ink overflow degree of the silver electrode. In Fig. 10(a)–(e), the blue wireframe represents the testing area, with a length of 200 μm and a width of 150 μm. The red line width represents the overflow area of ink. To measure the degree of ink overflow, the overflow degree can be defined by the following formula (3):

$$\text{Overflow degree} = \frac{A_o}{A_t} \times 100\% \quad (3)$$

where A_o is the overflow area of the ink, and A_t is the testing area.

At a moving acceleration of 25 mm s^{-2}, there was a significant amount of ink accumulation at the ends of the silver electrodes, leading to most of the electrode lines connecting. However, when the moving acceleration reached 40 mm s^{-2}, the ends of adjacent electrode lines were no longer connected. With the moving acceleration increasing, the overflow degree at the ends of the electrodes was significantly reduced from 39.8% to 4.3%. This meant that regulating the moving acceleration could significantly improve the ink overflow situation. Actually, the moving acceleration determined the residence time of the nozzle at the end of the electrode. The longer the time, the more ink would be ejected, resulting in a higher degree of ink overflow. In the actual production, the overflow area at the end of the electrode should be reduced as much as possible. By adjusting the moving acceleration, smaller scale ink accumulation area can be achieved.

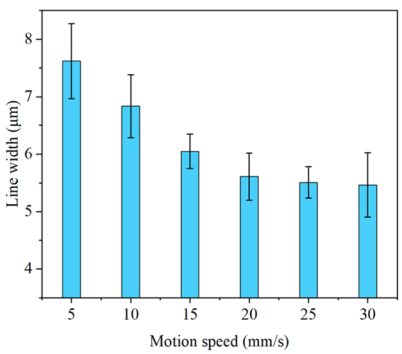

Fig. 9 The effect of movement speed on the line width of silver electrodes.

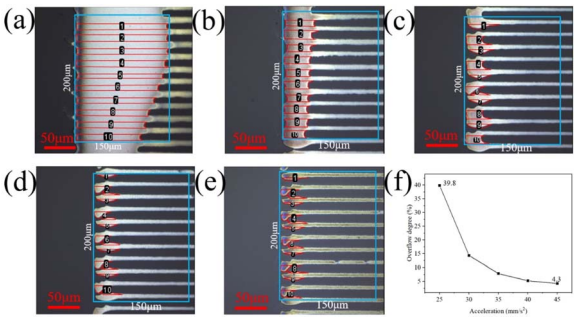

Fig. 10 The effect of acceleration on the ink accumulation degree of the silver electrode:(a) 25 mm s^2; (b) 30 mm s^2; (c) 35 mm s^2; (d) 40 mm s^2; (e) 45 mm s^2; (f) overflow degree.

3.3 Post treatment

Fig. 11(a) shows the *I–V* curves of the electrodes at different annealing temperatures. At an annealing temperature of 170–210 °C, the silver electrodes exhibited a typical linear resistance volt ampere characteristic curve. However, at an annealing temperature of 210 °C, the current on the silver electrode was almost 0 A, which shows that the electrode had a high resistivity. According to Ohm's law, the silver resistance was obtained by linear fitting of *I–V* curve. The electrode resistivity was calculated using the formula (2). Fig. 11(b) shows the resistivities of electrodes at different annealing temperatures. With the annealing temperature increasing, the resistivity of the silver electrodes decreased, and the value of resistivity uniformity also decreased. At an annealing temperature of 200 °C, the resistivity of the silver was 13.63 μΩ cm, with a resistivity uniformity value of 5.95%. This indicated that at this temperature, the electrical performance of the silver electrodes exhibited good reproducibility.

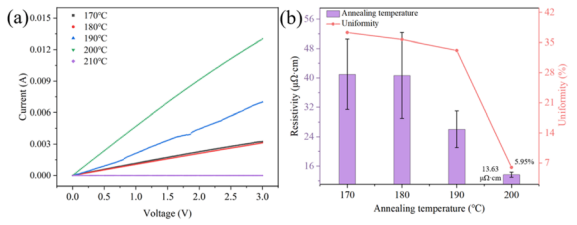

Fig. 11 Electrical performance of silver electrodes at different annealing temperatures: (a) *I–V* curve; (b) resistivity.

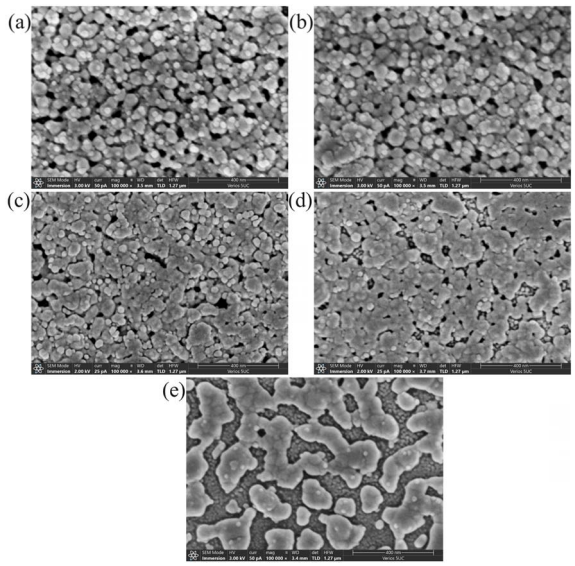

Fig. 12 SEM images of silver electrodes at different annealing temperatures: (a) 170 °C; (b) 180 °C; (c) 190 °C; (d) 200 °C; (e) 210 °C.

Fig. 12 shows the SEM images of silver electrodes at different annealing temperatures. At an annealing temperature of 170 °C, the overall fusion degree of silver nanoparticles was low, and the particles did not have tight contact with each other. This was because a significant amount of organic matter had yet to be removed at this temperature. With the annealing temperature increasing, the melting degree of silver nanoparticles increased, and the organic content gradually decreased. At an annealing temperature of 200 °C, the vast majority of silver nanoparticles fused into one piece with the minimal gaps. This led to the formation of high conductive silver film, which explained why the resistivity of silver electrode was the lowest at this temperature. However, when the annealing temperature reaches 210 °C, the silver particles fused into isolated particles, and the conductive channel of the silver electrode broke. This explained why the current of the silver electrode is almost 0 A at 210 °C.

Fig. 13(a) shows the carbon content in the silver electrodes tested by EDS. With the annealing temperature increasing, the carbon content gradually decreased, indicating that the residual organic matter gradually decreased. Fig. 13(b) shows the silver content in the silver electrodes. With the annealing temperature increasing, the silver content showed an increasing trend. At the annealing temperature of 200 °C, the silver content was approximately 38.81%. This increment of the silver content was also a factor affecting the reduction of resistivity of silver electrodes.

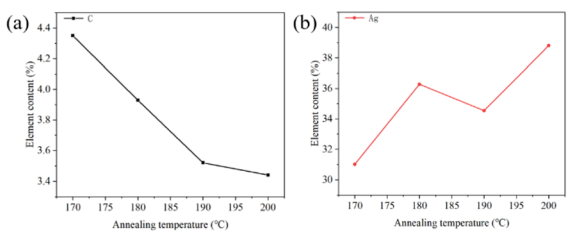

Fig. 13 Elemental content test results of silver electrodes at different annealing temperatures: (a) C element content; (b) Ag element content.

4. Conclusions

In this article, the relationship between the printing parameters and the morphology of silver electrode was investigated. With the driving voltage decreasing, the bias voltage decreasing and the moving speed increasing, the linewidth of the silver electrodes decreased. Silver electrodes with a line width of 3.85 μm were fabricated through process optimization, which is much narrower than the 10 μm linewidth electrode prepared by Ding. Y *et al.*[27] Besides, with the moving acceleration increasing, the degree of ink accumulation at the end of the electrode line reduced. Furthermore, with the annealing temperature increasing, the resistivity gradually decreased. The possible reason was that higher temperatures could not only increase the binding degree of silver nanoparticles, but also promote the removal of organic matter. Silver electrodes with a resistivity of 13.63 μΩ cm were fabricated through process optimization. In this article, the evaluation of the performance of printed electrodes is mainly limited to line width and resistivity, and there is a lack of evaluation of the adhesion between electrodes and substrates, long-term oxidation resistance, and other properties. In the future, EHD printed silver electrodes will be applied for performance verification in practical functional devices such as flexible OLED displays, thin-film transistors, and sensors.

Author contributions

Huacheng Tang: writing—original draft, investigation, data curation. Honglong Ning: writing—review and editing, funding acquisition. Rihui Yao: methodology. Zhenchao Li: investigation. Zhaohui Li: data curation. Zhenhuai Yang: investigation. Qi Lu: data curation. Qiang Hu: validation. Wei Xu: supervision. Junbiao Peng: supervision, methodology.

Conflicts of interest

There are no conflicts to declare.

Data availability

The data that support the findings of this study are available from the corresponding author upon reasonable request.

Acknowledgements

This work was supported by CUI CAN Program of Guangdong Province (No. CC/XM-202402ZJ0601), Key R&D Plan of Guangdong Province (2022B0303010001), National Natural Science Foundation of China (Grant no.62174057), Guangdong Natural Science Foundation (No.2024A1515012216 and No.2023A1515011026), Educational Commission of Guangdong Province (Grant no.2022ZDZX1002), State Key Lab of

Luminescent Materials and Devices (Skllmd-2025-07), Southwest Institute of Technology and Engineering Cooperation Fund (HDHDW59A020301) and Guangdong Basic Research Center of Excellence for Energy & Information Polymer Materials.

References

1 G. Kim, J. Yoon, H. Yoon, H. Cho, J. Seo and Y. Hong, *Flexible Printed Electron.*, 2022, **7**(4), 045009.
2 B. Li, W. Liang and F. Ren, *J. Mater. Sci. Mater. Electron.*, 2022, **33**(23), 18734–18750.
3 Y. Huang, N. Bu, Y. Duan, Y. Pan, H. Liu, Z. Yin and Y. Xiong, *Nanoscale*, 2013, **5**(24), 12007–12017.
4 Y. Yang, S. Gu, J. Liu, H. Tian and Q. Lv, *Micromachines*, 2018, **9**(11), 554.
5 N. Mkhize and H. Bhaskaran, *Small Sci.*, 2022, **2**(2), 2100073.
6 O. Yogi, T. Kawakami and A. Mizuno, *J. Electrost.*, 2006, **64**(7–9), 634–638.
7 J. Luo, Z. Ren, X. Qi, Q. Pan, D. Li, Y. Xiong, J. Yao, H. Liu, S. Yu and J. Wei, *Adv. Sci.*, 2025, 2414122.
8 C. Cong, X. Li, W. Xiao, J. Li, M. Jin, S. H. Kim and P. Zhang, *Nanotechnol. Rev.*, 2022, **11**(1), 3305–3334.
9 Z. Cui, Y. Han, Q. Huang, J. Dong and Y. Zhu, *Nanoscale*, 2018, **10**(15), 6806–6811.
10 X. Zheng, M. Hu, Y. Liu, J. Zhang, X. Li, X. Li and H. Yang, *Sci. China Mater.*, 2022, **65**(8), 2089–2109.
11 Q. Hao, J. Schossig, A. Towolawi, K. Xu, E. Bayiha, M. Mohanakanthan, D. Savastano, D. Jayaraman, C. Zhang and P. Lu, *ACS Appl. Eng. Mater.*, 2024, **2**(10), 2454–2467.
12 M. Magnani and M. Gamero-Castaño, *J. Fluid Mech.*, 2023, **972**, A34.
13 Z. Chen, X. Wang, L. Yin and Zhang, J Analysis and Research Based on Electrohydrodynamic Inkjet Printing, In *2024 21st China International Forum on Solid State Lighting & 2024 10th International Forum on Wide Bandgap Semiconductors (SSLCHINA: IFWS)*, 2024, vol. 18, pp. 1–4.
14 D. Gao, D. Yao, S. K. Leist, Y. Fei and J. Zhou, *Int. J. Bioprint.*, 2018, **5**(1), 166.
15 S. Cai, Y. Sun, Z. Wang, W. Yang, X. Li and H. Yu, *Nanotechnol. Rev.*, 2021, **10**(1), 1046–1078.
16 B. W. An, K. Kim, H. Lee, S. Y. Kim, Y. Shim, D. Y. Lee, J. Song and J. U. Park, *Adv. Mater.*, 2015, **27**(29), 4322–4328.
17 Y. H. Wang, D. X. Du, H. Xie, X. B. Zhang, K. W. Lin, K. Wang and E. Fu, *J. Mater. Sci. Mater. Electron.*, 2021, **32**(1), 496–508.
18 T. Kirscht, L. Jiang, F. Liu, X. Jiang, M. Marander, R. Ortega, H. Qin and S. Jiang, *ACS Appl. Mater. Interfaces*, 2024, **16**(33), 44225–44235.
19 T. T. T. Can, T. C. Nguyen and W. S. Choi, *Sci. Rep.*, 2019, **9**(1), 9180.
20 T. T. Rahman, M. S. Arman, V. Perez, B. Xu and J. Li, *Int. J. Adv. Des. Manuf. Technol.*, 2021, **115**(7), 2037–2047.
21 Z. Qiu, H. Zhu, Y. Wang, A. Kasimu, D. Li and J. He, *Bio-Des. Manuf.*, 2023, **6**(2), 136–149.
22 J. Zhang, M. Ahmadi, G. Fargas, N. Perinka, J. Reguera, S. Lanceros-Méndez, L. Llanes and E. Jiménez-Piqué, *Metals*, 2022, **12**(2), 234.
23 Y. Nomura, I. Amemiya, K. Mori, I. Takasu, K. Sugi and S. Uchikoga, High-Viscosity Electronic Materials Printing Using Ultrasonic Inkjet System, In, *NIP & Digital Fabrication Conference*, Society of Imaging Science and Technology, 2007, Vol. 23, pp. 859–862.
24 R. M. Gadirov, A. V. Odod, G. Y. Nazarova, A. E. Kurtsevich and T. N. Kopylova, *Russ. Phys. J.*, 2019, **61**(10).
25 Q. Lei, J. He, B. Zhang, J. Chang and D. Li, *J. Mater. Chem. C*, 2018, **6**(2), 213–218.
26 H. Liang, R. Yao, G. Zhang, X. Zhang, Z. Liang, Y. Yang, H. Ning, J. Zhong, T. Qiu and J. Peng, *Membranes*, 2022, **12**(2), 141.
27 Y. Ding, C. Xu, W. Zhang, Y. Di, J. Yue, K. Yu, W. Wang, D. Li and J. He, *Small*, 2025, **21**(12), 2410919.
28 B. Hwang and P. Matteini, *Coatings*, 2023, **13**(3), 617.
29 Y. Ishida, K. Sogabe, S. Kai and T. Asano, *Jpn. J. Appl. Phys.*, 2008, **47**(6S), 5281.
30 J. Kim, H. Oh and S. S. Kim, *J. Aerosol Sci.*, 2008, **39**(9), 819–825.
31 M. W. Lee, S. An, N. Y. Kim, J. H. Seo, J. Y. Huh, H. Y. Kim and S. S. Yoon, *Exp. Therm. Fluid Sci.*, 2013, **46**, 103–110.